metals

MDPI

Article

Preparation, Microstructure Evolutions, and Mechanical Property of an Ultra-Fine Grained Mg-10Gd-4Y-1.5Zn-0.5Zr Alloy

Huan Liu [1,2,*], Jia Ju [3], Jing Bai [4], Jiapeng Sun [1], Dan Song [1], Jingli Yan [4], Jinghua Jiang [1] and Aibin Ma [1,*]

1 College of Mechanics and Materials, Hohai University, Nanjing 211100, China; sunpengp@hhu.edu.cn (J.S.); songdancharls@hhu.edu.cn (D.S.); jinghua-jiang@hhu.edu.cn (J.J.)
2 Jiangsu Wujin Stainless Steel Pipe Group Company Limited, Changzhou 213111, China
3 College of Materials Engineering, Nanjing Institute of Technology, Nanjing 211167, China; materialju@njit.edu.cn
4 College of Materials Science and Engineering, Southeast University, Nanjing 211189, China; baijing@seu.edu.cn (J.B.); jlyan@seu.edu.cn (J.Y.)
* Correspondence: liuhuanseu@hhu.edu.cn (H.L.); aibin-ma@hhu.edu.cn (A.M.); Tel.: +86-025-8378-7239 (A.M.)

Received: 30 August 2017; Accepted: 25 September 2017; Published: 28 September 2017

Abstract: In this work, the microstructural evolutions and mechanical properties of an as-cast Mg-10Gd-4Y-1.5Zn-0.5Zr (wt %) alloy during successive multi-pass equal channel angular pressing (ECAP) were systematically investigated by X-ray diffractometer, scanning electron microscopy, transmission electron microscopy, and compression test. The obtained results show that the microstructure of as-cast alloy consists of α-Mg grains, Mg_3Gd island phase, few Y-rich particles, and lamellar 14H LPSO (long period stacking ordered) phase located at the grain boundaries. During ECAP, the Mg_3Gd-type phase is crushed and refined gradually. However, the refined Mg_3Gd particles are not distributed uniformly in the matrix, but still aggregated at the interdendritic area. The 14H phase becomes kinked during the early passes of ECAP and then broken at the kinking bands with more severe deformation. Dynamic recrystallization of α-Mg is activated during ECAP, and their average diameter decreases to around 1 μm, which is stabilized in spite of increasing ECAP passes. Moreover, nano-scale γ′ phases were dynamically precipitated in 16p ECAP alloy. Compression tests indicate that 16p ECAP alloy exhibits excellent mechanical property with compressive strength of 548 MPa and fracture strain of 19.1%. The significant improvement for both strength and ductility of deformed alloy could be ascribed to dynamic recrystallization (DRX) grains, refined Mg_3Gd-type and 14H particles, and dynamically precipitated γ′ plates.

Keywords: Mg-10Gd-4Y-1.5Zn-0.5Zr; long period stacking ordered phase; equal channel angular pressing; compression strength; fracture strain

1. Introduction

In recent years, with the increasing demands for light-weighting in the aerospace, high speed train, and automobile industries, magnesium and its alloys have received much attention due to their low density, high specific strength, and excellent damping capacities [1,2]. However, their inherent strengths are relatively lower when compared with steel and aluminum alloys, and lots of effort still need to be made to improve their strengths for broader applications [3,4].

Alloying with other elements—for example, Zn, Al, Mn, and so on [1,5]—is an important way to improve the strength of magnesium. The alloying elements can strengthen magnesium alloys by

second phase strengthening, solute solution strengthening, and precipitation strengthening [6,7]. Among various elements, heavy rare earth (HRE) elements, such as Gd and Y, are the most effective because they introduce severe lattice distortion when dissolved in α-Mg solid solution, and their solubility limits in α-Mg decline sharply with decreasing temperatures, which causes an obvious age-hardening response [8,9]. Moreover, by adding Zn and HRE elements simultaneously, a kind of novel long period stacking ordered (LPSO) structure is formed, which exhibits an extraordinary strengthening effect, especially in hot extruded or rolled Mg-RE-Zn alloys [10–12]. In addition, the LPSO phase can coexist with other Mg-RE second phases or precipitates and contributes to improving the mechanical properties of magnesium alloys together [13–17]. Therefore, multicomponent magnesium alloys with two or more HRE elements, such as Mg-Gd-Y-Zn series, usually display higher strength than ordinary Mg-RE-Zn ternary alloys [13,14]. Moreover, after aging treatment, due to the dense coherent β′ precipitates formed within α-Mg, the strengths of the β′/LPSO containing alloys could be significantly elevated further [16,17]. However, the ductility of these aged Mg-RE-Zn alloys is impaired [17].

Grain refinement is an effective strengthening strategy for conventional metals (Hall-Petch relationship), and it could also improve the plasticity of polycrystalline material at the same time [18]. But when grain size of metallic materials decreases to nanocrystalline (NS), the plasticity becomes relatively poor due to the limited dislocations movement in nanosized grains [19]. Therefore, ultra-fine grained (UFG) alloys with a grain size of 0.1–2 μm always exhibit combination of high strength and high ductility. Severe plastic deformation (SPD) is commonly used to fabricate bulk UFG metallic materials, and among various SPD techniques, equal channel angular pressing (ECAP) is one of the most popular methods that can refine the microstructures without changing shape of the materials [20,21]. Several studies have already been conducted on microstructure and property evolutions of LPSO-containing Mg-RE-Zn ternary alloys during ECAP [22–25]. Wu et al. [24] found that ECAP developed a bimodal microstructure with large deformed grains (Mg and LPSO) and sub-micron sized dynamically recrystallized (DRXed) grains in $Mg_{94}Y_4Zn_2$ (at %) alloy. Our previous study indicates that $Mg_{24}Y_5$ particles could also be dynamically precipitated during multi-pass ECAP of $Mg_{94}Y_4Zn_2$ alloy, and after 16 passes ECAP, the alloy displays excellent mechanical properties with compression strength of 611 MPa and fracture strain of 20.1% [25].

So far, little work has been reported on the ECAP processing of potential multicomponent Mg-Gd-Y-Zn alloys, and their microstructural evolutions would be more complicated than ternary alloys. Therefore, in this paper, the microstructure evolutions and mechanical properties of an UFG Mg-10Gd-4Y-1.5Zn-0.5Zr alloy via multi-pass successive ECAP were explored, which could provide a new prospect for developing of high strength and toughness Mg-RE based alloys.

2. Materials and Methods

Raw materials of pure metals Mg (99.95%), Zn (99.95%), and master alloys Mg-30Gd (wt %), Mg-30Y (wt %), and Mg-30Zr (wt %) were employed to prepare the cast Mg-10Gd-4Y-1.5Zn-0.5Zr (wt %) alloy. The melting process was performed in an electric resistance furnace (GR2, Hankou Furnace Company Ltd., Wuhan, China) under a protective atmosphere of CO_2 (1 vol %) and SF_6 (99 vol %) mixed gases. When the raw materials were molten, the melt was kept at 1023 K for 0.5 h, then they were poured into a water-cooling copper mold with a dimension of inner diameter of 60 mm and height of 200 mm. Afterward, cuboid samples with the dimension of 20 mm × 20 mm × 45 mm were cut from the central part of the ingot, and a rotational die ECAP (RD-ECAP) processing was then conducted on these samples. The schematic diagram for this RD-ECAP processing is listed in Figure 1, and it is apparent that multi-pass ECAP could be easily achieved by rotating the ECAP die without taking the sample out each pass [26]. The number of ECAP passes employed in this work were set as 1, 4, 8, 12 and 16, respectively. For each pass of ECAP, the processing temperature and extrusion speed were set as 633 K and 5 mm/min, respectively. Moreover, before the first pass and every four passes of ECAP, the sample was kept in the die and heated at 633 K for 10 min.

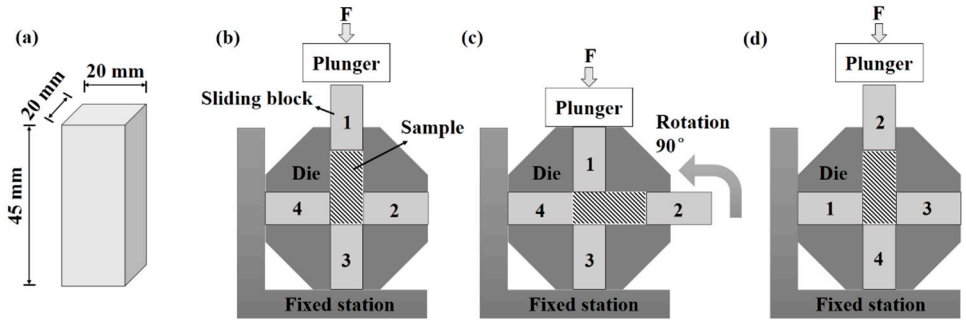

Figure 1. Schematic diagram to show the setup of rotational die (RD)-equal channel angular pressing (ECAP) processing: (**a**) Dimension of the ECAP sample; (**b**) initial state of first pass; (**c**) final state of first pass; (**d**) initial state of second pass.

Microstructure observations of the as-cast and ECAP alloys were carried out by an optical microscope (OM, Olympus BHM, Tokyo, Japan) and a scanning electron microscope (SEM, Field Electron and Ion Company, Hillsboro, OR, USA). The constituent phases of the alloy was identified by an X-ray diffractometer (XRD, D8 DISCOVER, Bruker, Billerica, MA, USA), a transmission electron microscope (TEM, Tecnai G2 20, Field Electron and Ion Company, Hillsboro, OR, USA), and an X-ray energy dispersive spectrometer (EDS, Field Electron and Ion Company, Hillsboro, OR, USA) equipped on SEM. Specimens for OM and SEM observations were mechanically ground, polished, and finally chemically etched with 4 mL nitric acid and 96 mL ethanol. For TEM examinations, the samples were twin-jet electron-polished and thinned, using a solution containing 5% perchloric acid and 95% ethanol. For the purpose of evaluating the mechanical properties, compression tests of cast and ECAP alloys were conducted by an electronic universal testing machine (CMT5105, MTS Systems Corporation, Eden Prairie, MN, USA) at the crosshead speed of 0.5 mm/min at room temperature. Compression specimens were derived from the center of ECAP samples, exhibiting a cylindrical shape with the diameter of 6 mm and height of 12 mm. Moreover, the axes of compression specimens are parallel to ECAP pressing direction, and three specimens were employed for each processing state.

3. Results and Discussions

3.1. Microstructure of As-Cast Alloy

Figure 2 shows the XRD pattern of as-cast alloy, and three phases are indexed from the corresponding diffraction peaks, which are α-Mg, Mg_3Gd, and $Mg_{12}YZn$ phases, respectively. The chemical formula $Mg_{12}YZn$ in XRD usually stands for the formation of LPSO phase, but it cannot be confirmed which type of LPSO phases is generated [27,28]. Figure 3a shows the optical micrograph of as-cast Mg-10Gd-4Y-1.5Zn-0.5Zr alloy. It is apparent that the alloy is composed of cellular α-Mg grains, and island-like phases located at intergranular regions. Moreover, some indistinct gray contrasts are also observed near second phases, which need to be identified further. Enlarged SEM image of as-cast alloy is shown in Figure 3b. Four obvious regions can be distinguished: eutectic phase I, lamellar phase II at the boundary of α-Mg grains, center of α-Mg phase III, and few cubic particles phase IV. To further explore the distributions of different elements, element mapping profiles were conducted and the results are shown in Figure 3c–g. It can been seen that the eutectic phases are enriched with solute atoms Gd, Y and Zn, and the cubic particle mainly consists of Y and Zr elements. Moreover, within α-Mg grains, Zn and Zr elements are uniformly distributed, but the rare-earth elements Gd and Y exhibit a little segregated near the eutectic phases.

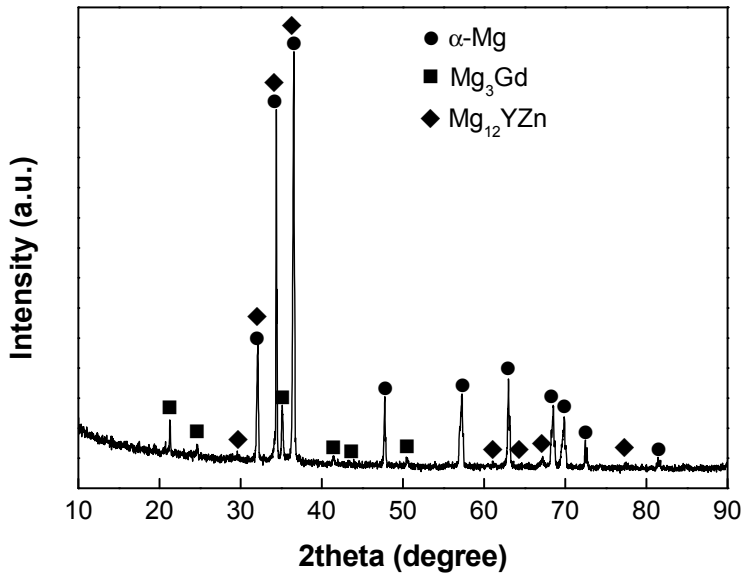

Figure 2. XRD pattern of as-cast alloy (XRD: X-Ray diffractometer).

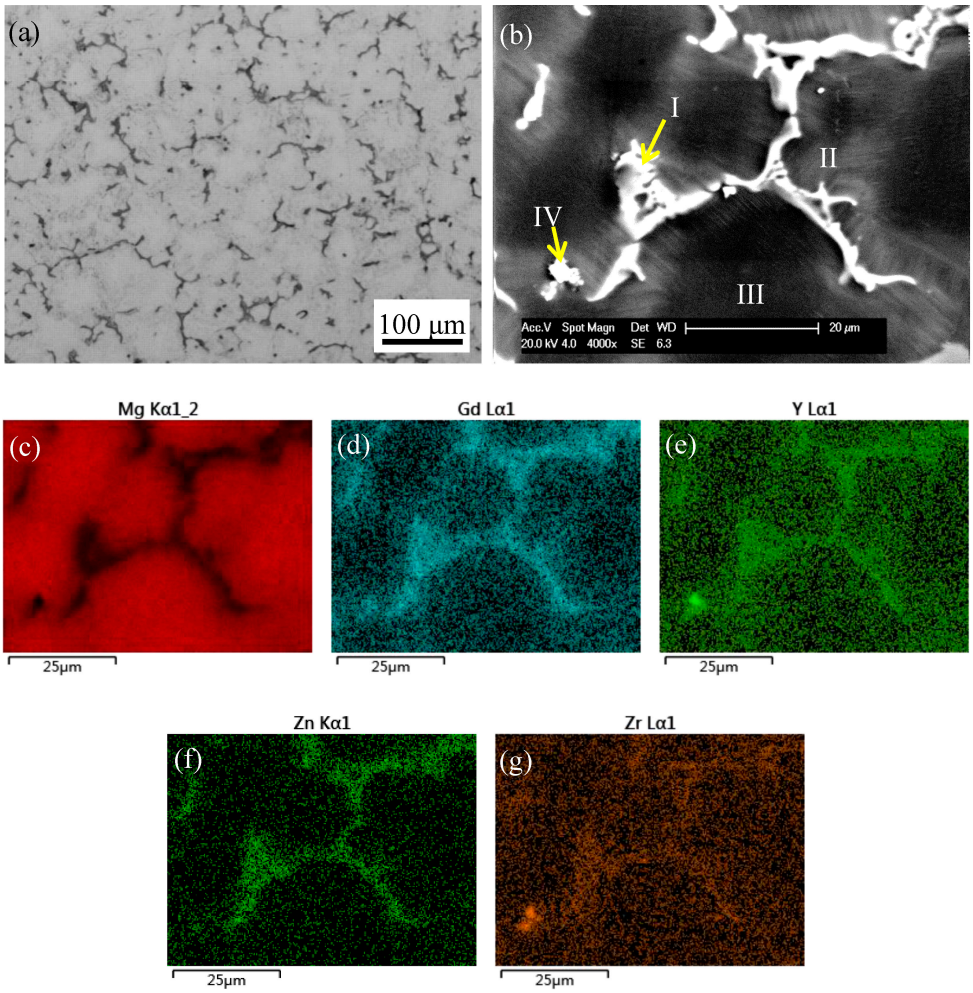

Figure 3. (**a**) Optical and (**b**) SEM (scanning electron microscope) micrographs of as-cast alloy with element map distributions of (**c**) Mg, (**d**) Gd, (**e**) Y, (**f**) Zn, and (**g**) Zr, respectively.

To identify various phases in Mg-10Gd-4Y-1.5Zn-0.5Zr alloy, EDS and TEM characterizations are performed. Figure 4 exhibits the EDS results of four regions marked in Figure 3b, which provides more quantitative information than the element map distributions. Combined with XRD patterns and EDS results, it can be confirmed that the eutectic phase I and lamellar phase II are Mg_3Gd-type and $Mg_{12}YZn$-type phases, respectively. Considering their analyzed compositions, it is more reasonable to depict their chemical formula as $Mg_3(Gd,Y,Zn)$ and $Mg_{12}(Gd,Y)Zn$.

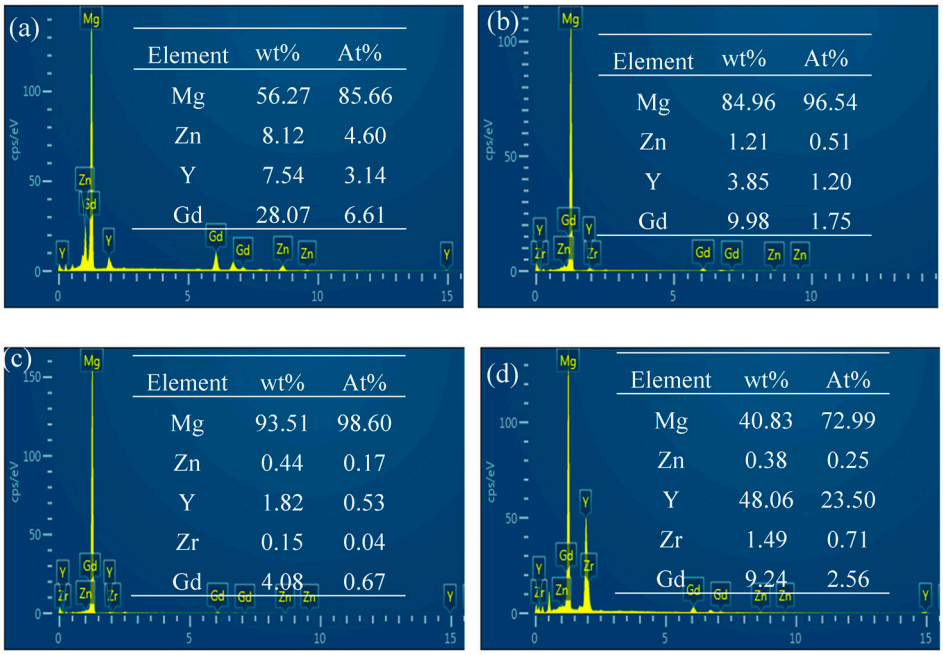

Figure 4. Analyzed chemical compositions of various areas marked in Figure 3b: (**a**) Area I; (**b**) area II; (**c**) area III; (**d**) area IV.

Figure 5a shows the TEM observation of an intergranular region, including a block of eutectic phase and plenty of lamellas. The corresponding selected area electron diffraction (SAED) pattern illustrated in Figure 5b further demonstrates the eutectic phase is Mg_3Gd-type phase [29]. Moreover, corresponding SAED pattern of lamellar phases listed in Figure 5c proves that they are 14H LPSO phase [27]. The structure of LPSO phase formed in cast alloy usually is 18R type for Mg-Y-Zn alloys, and is 14H LPSO for Mg-Gd-Zn alloys [30,31]. In this work, since the Gd content is much higher than Y element, the obtained LPSO phase in cast alloy obeys the rule of Mg-Gd-Zn series. In addition, the TEM image of Figure 5d illustrates the center region of α-Mg grains. Although no obvious lamellar phases can be observed, there exists some line contrast. The visible streaks located between diffraction spots in correspond SAED patterns of Figure 5e confirm the existence of stacking faults (SFs), and further investigation proves these SFs are on (0001) basal plane of α-Mg [32].

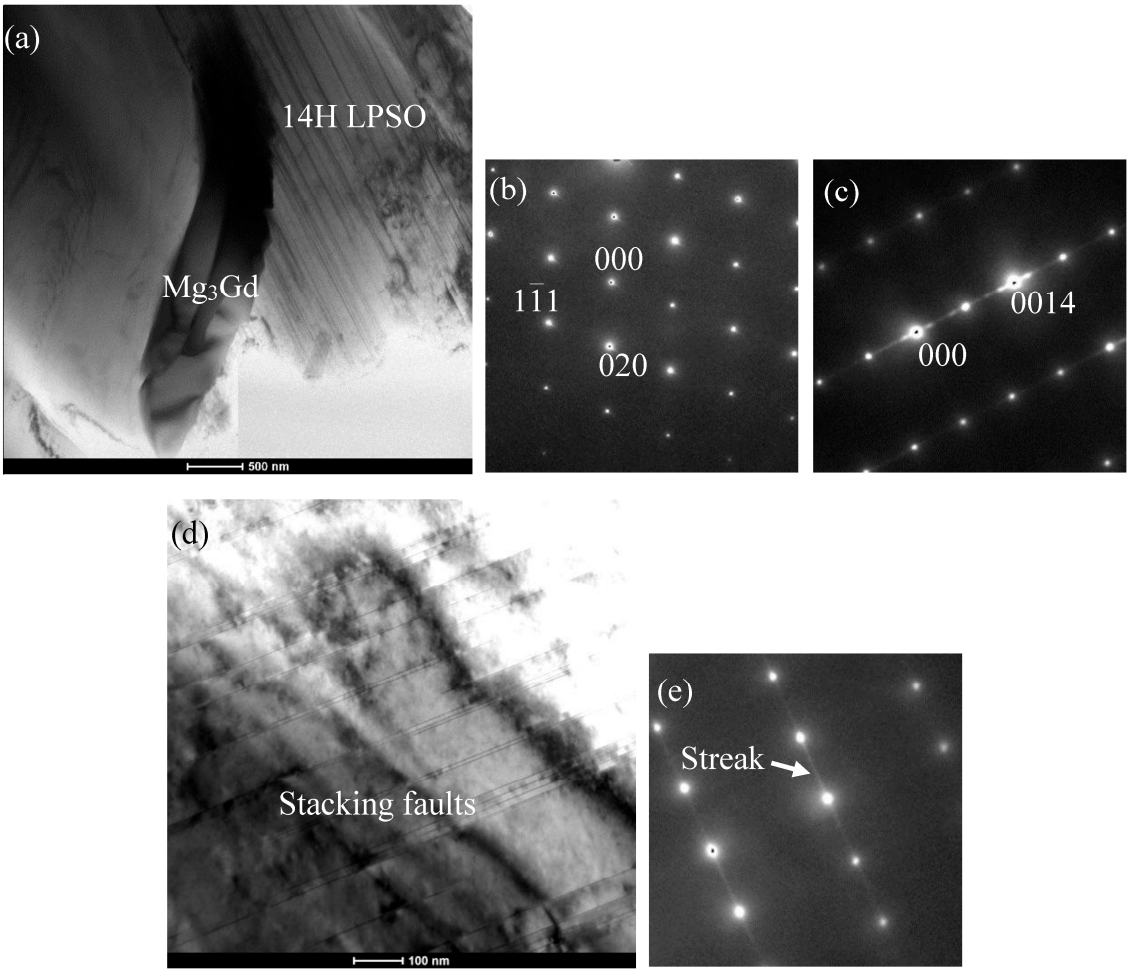

Figure 5. TEM (transmission electron microscope) micrographs of as-cast alloy: (**a**) Mg_3Gd phase and long period stacking ordered (LPSO) phase; selected area electron diffraction (SAED) patterns of (**b**) Mg_3Gd phase and (**c**) LPSO phase; (**d**) the center area of α-Mg grain and (**e**) its corresponding SAED pattern.

3.2. Microstructure of ECAP (Equal Channel Angular Pressing) Alloy

Figure 6 shows the microstructure evolutions of cast Mg-10Gd-4Y-1.5Zn-0.5Zr alloy during multi-pass ECAP. After one pass of ECAP, the island $Mg_3(Gd,Y,Zn)$ phase seems distorted and broken, but no other remarkable change is observed, as can be seen form Figure 6a. When the ECAP pass increases to four, the distortion degree of second phases is accelerated. In addition, finer dynamically recrystallized (DRXed) α-Mg grains were observed in 4p-ECAP alloy, which were not identified in 1p-ECAP alloy. This is because DRX is a process associated with both processing temperature and strains, and the accumulated energy becomes sufficient to activate DRX with more ECAP passes [33,34]. With further increase of ECAP passes, DRX proceeds continuously, and the second phases become finer. However, seen from Figure 6c, the refined second phases were not uniformly distributed within the whole matrix, but still gathered at intergranular regions. In ECAP alloy with sixteen passes (Figure 6d), although the DRX region and the intergranular region with particles can still be distinguished obviously, its microstructure becomes more uniform than other alloys with lower ECAP passes in this work. It is reasonable to believe that with further increased ECAP passes, the refined particles will finally be mixed with DRX grains.

To further investigate the evolutions of various phases, high-magnification observations of the microstructure were conducted, and typical SEM images are exhibited in Figure 7. Figure 7a displays

the as cast microstructure, and it is apparent that three $Mg_3(Gd,Y,Zn)$ blocks, an α-Mg grain without 14H lamellas, and several α-Mg grains with plenty of 14H lamellas are confirmed. The 14H in cast alloy exhibits straight lamellar shape and they are parallel with each other in the same grain, but with diverse orientations in different grains, which is attributed to their fixed orientation relationship with α-Mg phase [27]. Moreover, the 14H is not formed uniformly in all grains. Its generation involves two factors, formation of plenty of SFs, and sufficient solute atoms to orderly diffuse into SFs [35]. In regions where these two factors are satisfied, 14H can propagate rapidly. Therefore, the observed α-Mg grain without 14H in Figure 7a could result from either lack of SFs or depletion of solute atoms.

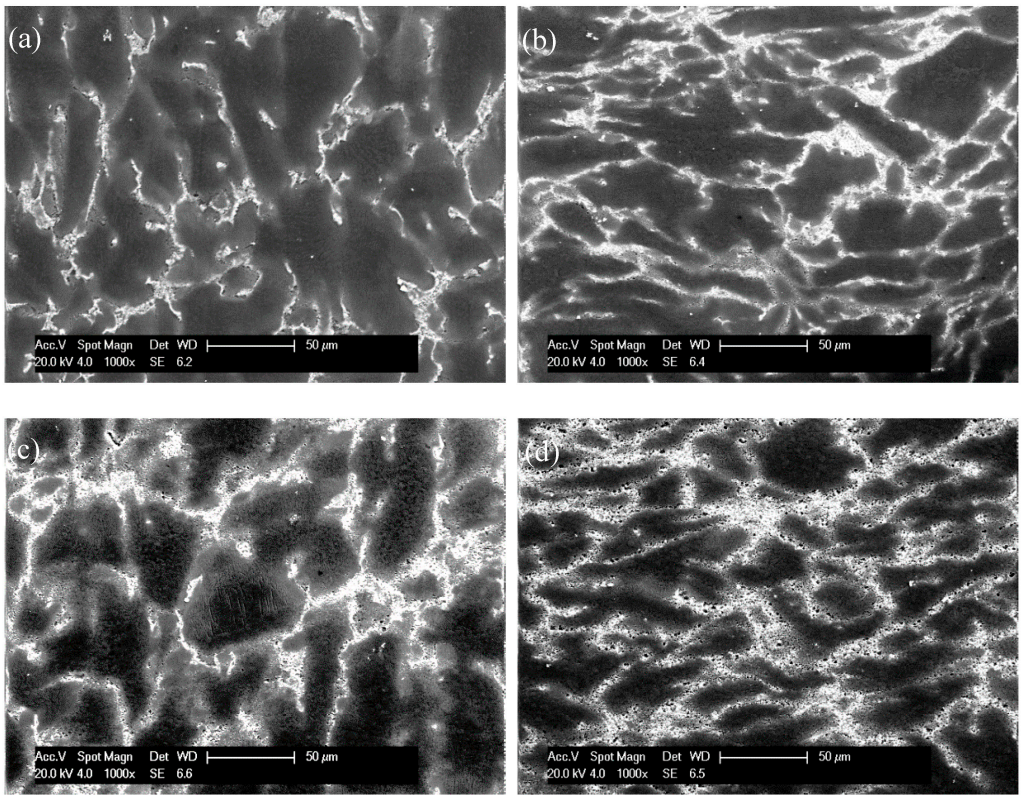

Figure 6. SEM images of ECAP alloys: (**a**) 1p; (**b**) 4p; (**c**) 8p; (**d**) 16p.

As shown in Figure 7b, the $Mg_3(Gd,Y,Zn)$ block was crashed but not broken into pieces after only one pass ECAP. In addition, the 14H lamellas became bent, which is caused by kinking. Kinking was considered as the dominated deformation mechanism for lamellar LPSO structures, as the main slip system could be easily hindered during deformation [34,36]. After four passes of ECAP, it can be seen from Figure 7c that a mixed area was generated at intergranular regions. The mixed area usually consists of plenty of finer $Mg_3(Gd,Y,Zn)$ particles, DRX grains, and small 14H clusters. Marked by Arabic numbers in Figure 7c, four small 14H clusters with diameter range of 2–5 μm were surrounded by particles or DRX grains. Compared with 14H in cast and 1p-ECAP samples, the size of these 14H cluster is much smaller, suggesting refining of 14H happens during ECAP. In our former work, we have proved that the refining process of 14H LPSO was caused by kinkings at different shear direction [33]. As dislocations are generated in kinking bands, 14H becomes cracked as long as the number of tangled dislocations reach the maximum. Moreover, seen from Figure 7d, with increased ECAP passes, although mixed areas are widely developed at intergranular regions and propagate into α-Mg region gradually, there still exist clean DRX regions where 14H and $Mg_3(Gd,Y,Zn)$ particles are absent. In addition, the average diameter of DRX grains was estimated to be around 1 μm, suggesting the effective refining effect of multi-pass RD-ECAP employed in this work.

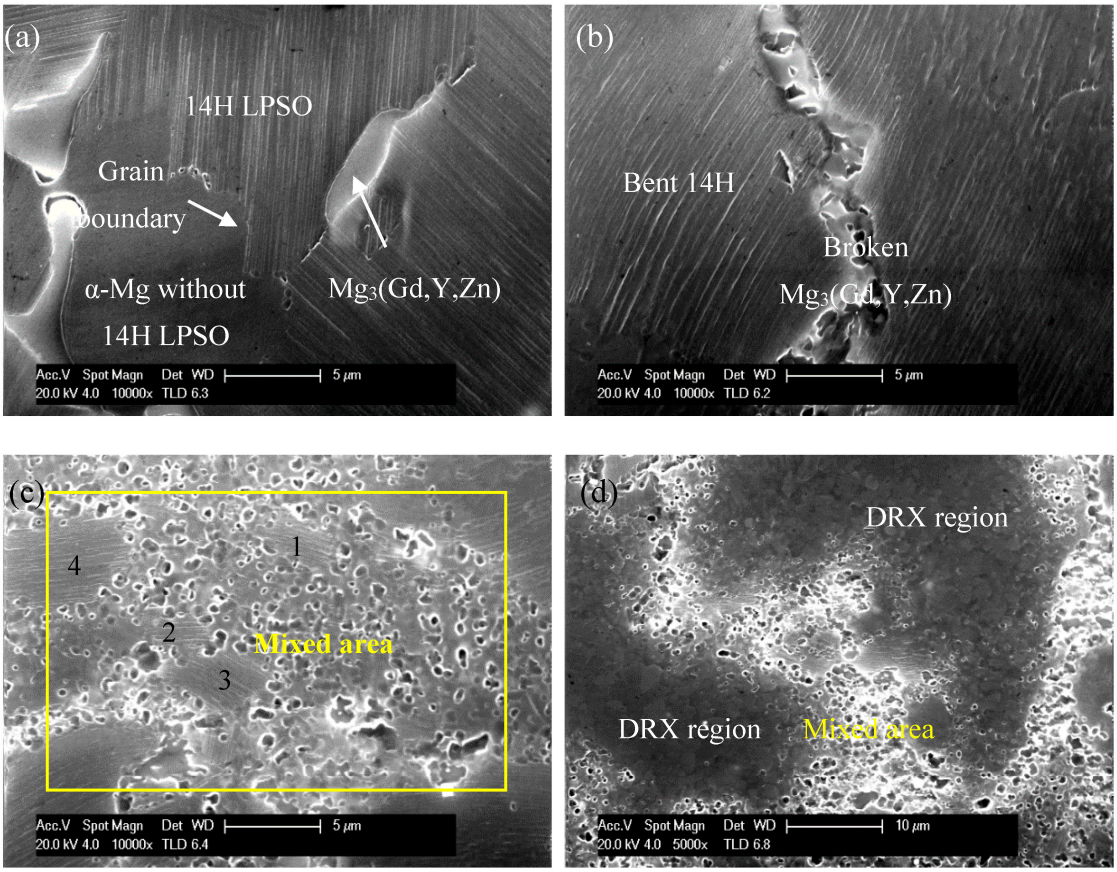

Figure 7. Typical SEM images showing the evolutions of various phases: (**a**) Cast alloy; (**b**) 1p ECAP; (**c**) 4p ECAP; (**d**) 12p ECAP (DRX: Dynamic recrystallization).

Figure 8a illustrates the TEM image of $Mg_3(Gd,Y,Zn)$ particles in 12p-ECAP sample. It can be seen that the $Mg_3(Gd,Y,Zn)$ phases are obviously refined after ECAP, and their average diameter is around 0.5 μm. In addition, Figure 8b displays the TEM observation of a mixed area which is shown in Figure 7c. Apart from the refined $Mg_3(Gd,Y,Zn)$ particles, refined 14H phase and DRX grains are also observed. It is widely acknowledged that the hard particles could promote DRX process through a particle-stimulated nucleation (PSN) mechanism [37]. In this work, both the $Mg_3(Gd,Y,Zn)$ particles and LPSO phase are harder than α-Mg, and they could act as nuclei for DRX, especially when they are refined into particles in submicron range. Seen from Figure 8b, several DRX grains are surrounded by 14H and $Mg_3(Gd,Y,Zn)$ particles [20]. The formation of these DRX grains could be caused by the interaction between 14H and dislocations. Since the elastic modulus of LPSO phase is much larger than α-Mg matrix, the deformation of 14H and α-Mg phases during ECAP will not be coordinated, and dislocations are accumulated at 14H/α-Mg interfaces [37]. As the number of dislocations increases at the interface, the dislocations are tangled and turn into sub-boundaries, and finally, a DRX grain is generated. Moreover, Figure 8c shows a DRX α-Mg grain with diameter of 0.7 μm, and it is apparent that a cluster of 14H lamellas locates within this grain, and both ends of the cluster are stopped at the grain boundary. This 14H lamella might be dynamically precipitated after DRX is formed during ECAP, as the processing temperature and severe deformation could provide requirement for generation of LPSO phase [33,35]. However, the detailed information concerning the relationship between DRX and dynamic precipitation of 14H is still unclear, and our further will focus on this issue.

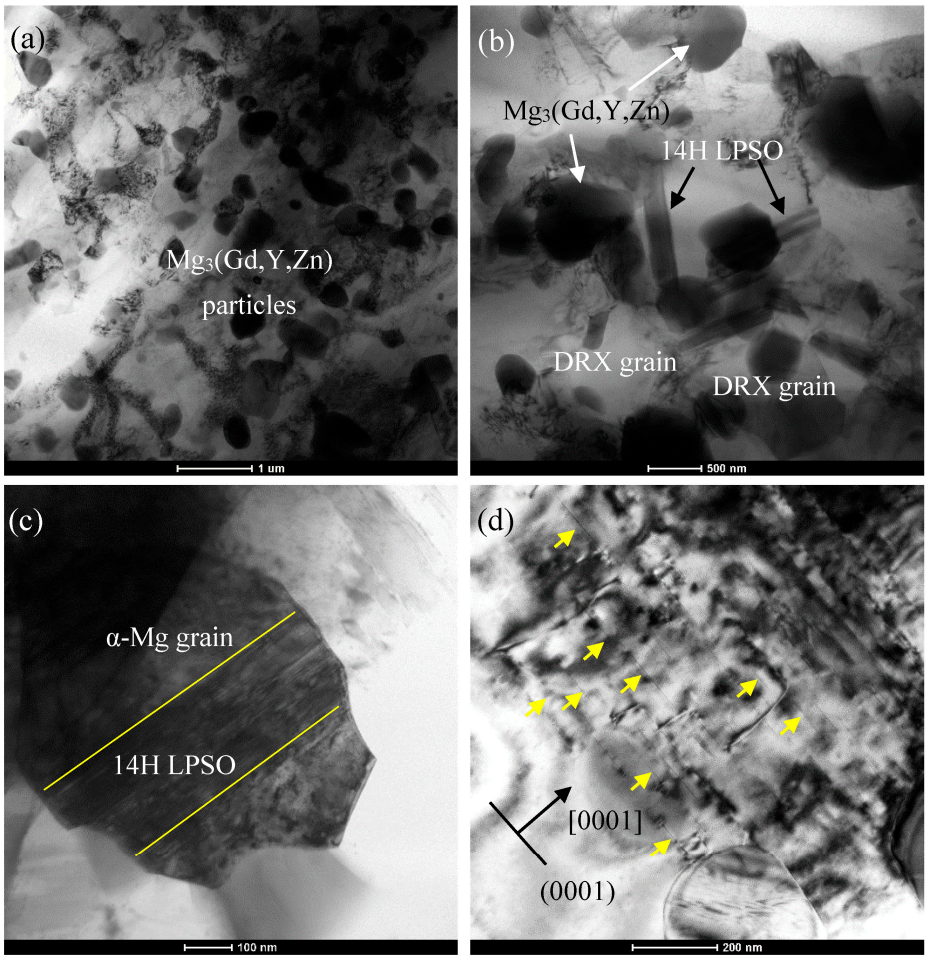

Figure 8. TEM images of ECAP alloys: (**a**) Refined Mg_3(Gd,Y,Zn) particles; (**b**) mixed area in Figure 7c; (**c**) an α-Mg grain with a 14H cluster inside (the 14H phase is located within two yellow lines); (**d**) γ′ precipitates formed in 16p-ECAP alloy (some γ′ precipitates are marked by yellow arrows).

Furthermore, shown in Figure 8d, a kind of plate-shape precipitation is precipitated in 16p-ECAP alloy. The lengths of these precipitates are in the range of 100–200 nm, and their thickness is several nanometers. Further investigation suggests they are precipitates on (0001) basal planes of α-Mg. These precipitates are identified as γ′ phases, which were reported in Mg-Gd-Zn alloys when these alloys are subjected to aging at 200 °C [38,39]. The precipitation sequence for Mg-RE (Gd or Y) alloys are usually recognized as SSSS (super-saturated solid solution) → β″ (hcp, D019) → β′ (cbco) → β1 (fcc) → β (fcc) [16,17]. However, for Mg-Gd-Zn systems, recent studies indicate an additional precipitation sequence formed on basal plane of α-Mg as SSSS→γ″ (ordered hcp) → γ′ (hcp) [40]. For the ECAP alloys in this work, γ′ precipitates were only found in 16p-ECAP alloy, but were not observed in other ECAP alloys with lower passes. This is because the precipitation of γ′ phase needs thermal activation energy to nucleate and grow. Although the temperature of ECAP is much higher than usual aging temperature, the processing time employed here is short, which could not provide sufficient energy for the generation of γ′ phase when ECAP pass is low.

3.3. Mechanical Properties of Cast and ECAP Alloys

The compression engineering stress-strain curves of cast and ECAP alloys are presented in Figure 9a. Moreover, the variations of compression yield strength, compression strength, and fraction strain with ECAP passes are also summarized in Figure 9b. The yield strength and compression

strength for the alloy after one pass of ECAP increased to 234.8 MPa and 442.6 MPa when compared with 182.6 MPa and 363.4 MPa for cast alloy. Afterward, the compression strength of the alloy increases steadily with ECAP passes, and the alloy with 16p-ECAP exhibits the highest strength of 548.2 MPa. However, as for yield strength, it displays a fluctuant variation with number of ECAP pass. During early passes, the compression yield strength grows continuously and reaches a maximum value after eight passes ECAP. Afterward, it decreases slightly after 12 passes and then continues to increase after 16 passes. These results show that the compression yield strength might be stabilized at 300 MPa approximately with further ECAP passes, as the microstructure refining effect would reach a saturation level. In addition, although the fraction strain decreases after four passes of ECAP, it continues to go up with further increasing ECAP numbers, and the alloy with the highest ECAP passes displays a fraction strain of 19.1%. Based on above considerations, it can be concluded that 16p-ECAP alloy exhibits the best comprehensive mechanical properties with both highest strength and ductility. In addition, it is reasonable to believe that with further increase of ECAP passes, the mechanical properties could be improved further, and finally a steady strength value should be reached.

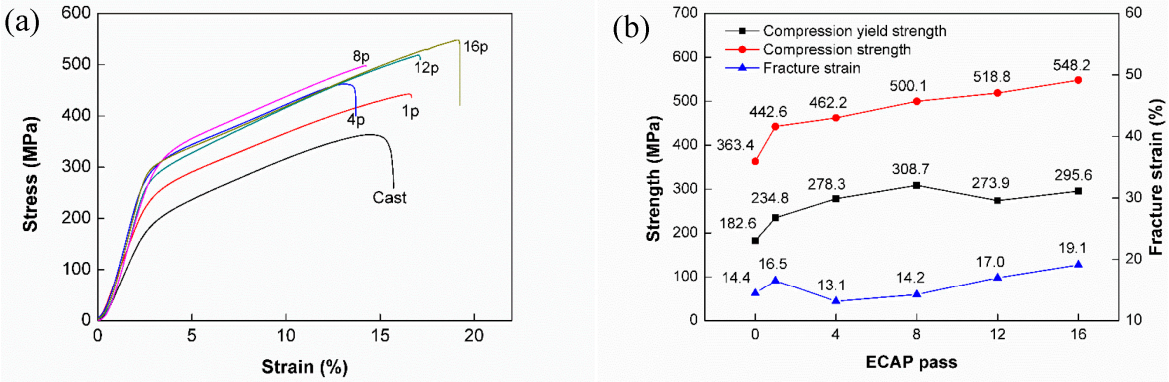

Figure 9. Mechanical properties of cast and ECAP alloys: (**a**) Typical compression engineering stress–strain curves; (**b**) variations of compression yield strength, compression strength and fracture strain with ECAP passes.

Strengthening of the ECAP alloy in this work is mainly ascribed to refinement of the microstructures. During the former passes of ECAP, $Mg_3(Gd,Y,Zn)$ phase was refined into small particles, but DRX was not activated yet, and the 14H lamellas were bent and kinked. In this early ECAP stage, the strengthening effect originates from refined $Mg_3(Gd,Y,Zn)$ particles and kinkings of 14H LPSO phase [34]. With further increase of ECAP pass, on the one hand, as the kinking degree was accelerated, bent 14H lamellas broke during kinking bands and transform into fine particles in submicron range. On the other hand, DRX is activated through a PSN mechanism owing to the hard second phase particles [37], and the newly formed DRX grains exhibit an average grain size near 1 μm. Therefore, in the medium-term ECAP stage, refined microstructures of $Mg_3(Gd,Y,Zn)$ particles, 14H microcells and DRX grains contribute to strengthening of the UFG alloy together. When the ECAP pass increases to 16, the uniformity of the refined microstructures was improved. In addition, a kind of coherent nano-scale γ' phases were precipitated within α-Mg grains. It has been reported that the γ' precipitates are more beneficial for the strength improvement than LPSO phase [38]. Therefore, combined with refined microstructures and dynamically precipitated γ' nanoparticles, the 16p-ECAP alloy exhibit the highest strength.

Moreover, it can be seen from the engineering stress-strain curves that the ECAP alloy in this work display strong work hardening effect, which suggests that the interaction between dislocations and microstructures (refined second phases, grain boundaries, and nano-precipitates) plays an important role in strengthening of the alloys [41]. The refined microstructures and increased phase boundaries or

grain boundaries are effective to hinder the propagation of micro cracks, which obviously improves the toughness of the ECAP alloys.

4. Conclusions

The microstructure evolutions and mechanical properties of Mg-10Gd-4Y-1.5Zn-0.5Zr (wt %) alloy during multi-pass RD-ECAP were systematically investigated, and a high strength and toughness UFG magnesium alloy was fabricated in this work. The main conclusions could be summarized as follows:

(1) The microstructure of as-cast Mg-10Gd-4Y-1.5Zn-0.5Zr alloy consists of α-Mg grains, island-like Mg_3(Gd,Y,Zn) phases and 14H LPSO lamellas. The 14H lamellas are usually located within α-Mg near the boundaries of Mg_3(Gd,Y,Zn) phase.

(2) The Mg_3(Gd,Y,Zn) blocks were broken into fine particles (0.5 μm) gradually during multi-pass ECAP. 14H lamellas were bent first, and then transformed into fine particles in submicron range. With ECAP pass number increasing, DRX was activated by fine particles through PSN mechanism. Moreover, nano-scale γ′ phases were dynamically precipitated in 16p-ECAP alloy.

(3) The 16p-ECAP alloy exhibits excellent comprehensive mechanical properties with compression strength of 548.2 MPa and fracture strain of 19.1%. The significant improvement for both strength and toughness could be ascribed to strengthening of the ultra-fine grained DRX α-Mg, refined Mg_3(Gd,Y,Zn) and 14H particles, and dynamically precipitated γ′ nanoparticles.

Acknowledgments: This work was supported by the Natural Science Foundation of Jiangsu Province of China (No. BK20160869), the China Postdoctoral Science Foundation (No. 2017M611671), the Fundamental Research Funds for the Central Universities (No. 2015B01314 and No. 2016B10314), and the Key Research and Development Project of Jiangsu Province of China (No. BE2017148).

Author Contributions: Huan Liu and Aibin Ma conceived and designed the experiments; Huan Liu and Jia Ju performed the experiments; Jing Bai and Jingli Yan contributed materials; Jiapeng Sun and Dan Song analyzed the data; Huan Liu and Jinghua Jiang wrote the paper. All authors have discussed the results, read and approved the final manuscript.

Conflicts of Interest: The authors declare no conflict of interest.

References

1. Pan, F.S.; Yang, M.B.; Chen, X.H. A review on casting magnesium alloys: Modification of commercial alloys and development of new alloys. *J. Mater. Sci. Technol.* **2016**, *32*, 1211–1221. [CrossRef]
2. Liu, W.; Zhang, J.S.; Wei, L.Y.; Xu, C.X.; Zong, X.M.; Hao, J.Q. Extensive dynamic recrystallized grains at kink boundary of 14H LPSO phase in extruded $Mg_{92}Gd_3Zn_1Li_4$ alloy. *Mater. Sci. Eng. A* **2017**, *681*, 97–102. [CrossRef]
3. Liu, H.; Cheng, Z.J.; Yan, K.; Yan, J.L.; Bai, J.; Jiang, J.H.; Ma, A.B. Effect of multi-pass equal channel angular pressing on the microstructure and mechanical properties of a heterogeneous $Mg_{88}Y_8Zn_4$ alloy. *J. Mater. Sci. Technol.* **2016**, *32*, 1274–1281. [CrossRef]
4. Xu, D.K.; Han, E.H.; Xu, Y.B. Effect of long-period stacking ordered phase on microstructure, mechanical property and corrosion resistance of Mg alloys: A review. *Prog. Nat. Sci. Mater. Int.* **2016**, *26*, 117–128. [CrossRef]
5. Wang, Y.; Rong, W.; Wu, Y.J.; Peng, L.M.; Chen, J.; Ding, W.J. Effects of Mn addition on the microstructures and mechanical properties of the Mg-15Gd-1Zn alloy. *J. Alloys Compd.* **2017**, *698*, 1066–1076. [CrossRef]
6. Tekumalla, S.; Seetharaman, S.; Almajid, A.; Gupta, M. Mechanical properties of magnesium-rare earth alloy systems: A review. *Metals* **2015**, *5*, 1–39. [CrossRef]
7. Dini, H.; Andersson, N.E.; Jarfors, A.E.W. Effect of $Mg_{17}Al_{12}$ fraction on mechanical properties of Mg-9%Al-1%Zn cast alloy. *Metals* **2016**, *6*, 251. [CrossRef]
8. Wang, J.F.; Song, P.F.; Huang, S.; Pan, F.S. High-strength and good-ductility Mg-RE-Zn-Mn magnesium alloy with long-period stacking ordered phase. *Mater. Lett.* **2013**, *93*, 415–418. [CrossRef]
9. Zhang, J.S.; Zhang, W.B.; Bian, L.P.; Cheng, W.L.; Niu, X.F.; Xu, C.X.; Wu, S.J. Study of Mg-Gd-Zn-Zr alloys with long period stacking ordered structures. *Mater. Sci. Eng. A* **2013**, *585*, 268–276. [CrossRef]

10. Li, Z.L.; Liu, F.; Yuan, A.P.; Duan, B.Y.; Li, Y.M.; Li, X.W. Effect of rolling deformation on microstructure and texture of spray-deposited magnesium alloy containing Mg-Nd-Zn typed LPSO. *J. Mater. Sci. Technol.* **2017**, *33*, 630–636. [CrossRef]
11. Liu, X.; Zhang, Z.Q.; Hu, W.Y.; Le, Q.C.; Bao, L.; Cui, J.Z. Effects of extrusion speed on the microstructure and mechanical properties of Mg-9Gd-3Y-1.5Zn-0.8Zr alloy. *J. Mater. Sci. Technol.* **2016**, *32*, 313–319. [CrossRef]
12. Itoi, T.; Inazawa, T.; Yamasaki, M.; Kawamura, Y.; Hirohashi, M. Microstructure and mechanical properties of Mg-Zn-Y alloy sheet prepared by hot-rolling. *Mater. Sci. Eng. A* **2013**, *560*, 216–223. [CrossRef]
13. Xu, C.; Nakata, T.; Qiao, X.G.; Zheng, M.Y.; Wu, K.; Kamado, S. Effect of LPSO and SFs on microstructure evolution and mechanical properties of Mg-Gd-Y-Zn-Zr alloy. *Sci. Rep.* **2017**, *7*, 40846. [CrossRef] [PubMed]
14. Sun, W.T.; Xu, C.; Qiao, X.G.; Zheng, M.Y.; Kamado, S.; Gao, N.; Starink, M.J. Evolution of microstructure and mechanical properties of an as-cast Mg-8.2Gd-3.8Y-1.0Zn-0.4Zr alloy processed by high pressure torsion. *Mater. Sci. Eng. A* **2017**, *700*, 312–320. [CrossRef]
15. Jiang, H.S.; Qiao, X.G.; Xu, C.; Zheng, M.Y.; Wu, K.; Kamado, S. Ultrahigh strength as-extruded Mg-10.3Zn-6.4Y-0.4Zr-0.5Ca alloy containing W phase. *Mater. Des.* **2016**, *108*, 391–399. [CrossRef]
16. Yin, D.D.; Wang, Q.D.; Gao, Y.; Chen, C.J.; Zheng, J. Effects of heat treatments on microstructure and mechanical properties of Mg-11Y-5Gd-2Zn-0.5Zr (wt %) alloy. *J. Alloys Compd.* **2011**, *509*, 1696–1704. [CrossRef]
17. Liu, H.; Xue, F.; Bai, J.; Sun, Y.S. Effect of heat treatments on the microstructure and mechanical properties of an extruded $Mg_{95.5}Y_3Zn_{1.5}$ alloy. *Mater. Sci. Eng. A* **2013**, *585*, 261–267. [CrossRef]
18. Hu, J.; Shi, Y.N.; Sauvage, X.; Sha, G.; Lu, K. Grain boundary stability governs hardening and softening in extremely fine nanograined metals. *Science* **2017**, *6331*, 1292–1296. [CrossRef] [PubMed]
19. Lu, K. Stabilizing nanostructures in metals using grain and twin boundary architectures. *Nat. Rev. Mater.* **2016**, *1*, 16019. [CrossRef]
20. Valiev, R.Z.; Longdon, T.G. Principles of equal-channel angular pressing as a processing tool for grain refinement. *Prog. Mater. Sci.* **2006**, *7*, 881–981. [CrossRef]
21. Wei, J.; Huang, G.H.; Yin, D.D.; Li, K.N.; Wang, Q.D.; Zhou, H. Effects of ECAP and annealing treatment on the microstructure and mechanical properties of Mg-1Y (wt %) binary alloy. *Metals* **2017**, *7*, 119. [CrossRef]
22. Lapovok, R.; Gao, X.; Nie, J.F.; Estrin, Y.; Mathaudhu, S.N. Enhancement of properties in cast Mg-Y-Zn rod processed by severe plastic deformation. *Mater. Sci. Eng. A* **2014**, *615*, 198–207. [CrossRef]
23. Chen, B.; Lin, D.L.; Zeng, X.Q.; Lu, C. Microstructure and mechanical properties of ultrafine grained $Mg_{97}Y_2Zn_1$ alloy processed by equal channel angular pressing. *J. Alloys Compd.* **2007**, *440*, 94–100. [CrossRef]
24. Wu, J.; Shi, Q.; Ma, H.C.; Chiu, Y.L. Microstructure and mechanical behaviour of a $Mg_{94}Zn_2Y_4$ alloy processed by equal channel angular pressing. *Mater. Sci. Eng. A* **2016**, *669*, 417–427. [CrossRef]
25. Liu, H.; Ju, J.; Lu, F.M.; Yan, J.L.; Bai, J.; Jiang, J.H.; Ma, A.B. Dynamic precipitation behavior and mechanical property of an $Mg_{94}Y_4Zn_2$ alloy prepared by multi-pass successive equal channel angular pressing. *Mater. Sci. Eng. A* **2017**, *682*, 255–259. [CrossRef]
26. Ma, A.B.; Suzuki, K.; Nishida, Y.; Saito, N.; Shigematsu, I.; Takagi, M.; Iwata, H.; Watazu, A.; Imura, T. Impact toughness of an ultrafine-grained Al–11mass%Si alloy processed by rotary-die equal-channel angular pressing. *Acta Mater.* **2005**, *53*, 211–220. [CrossRef]
27. Zhu, Y.M.; Morton, A.J.; Nie, J.F. Growth and transformation mechanisms of 18R and 14H in Mg-Y-Zn alloys. *Acta Mater.* **2012**, *60*, 6562–6572. [CrossRef]
28. Luo, Z.P.; Zhang, S.Q. High-resolution electron microscopy on the X-$Mg_{12}ZnY$ phase in a high strength Mg-Zn-Zr-Y magnesium alloy. *J. Mater. Sci. Lett.* **2000**, *19*, 813–815. [CrossRef]
29. Zhang, S.; Yuan, G.Y.; Lu, C.; Ding, W.J. The relationship between $(Mg,Zn)_3RE$ phase and 14H-LPSO phase in Mg-Gd-Y-Zn-Zr alloys solidified at different cooling rates. *J. Alloys Compd.* **2011**, *509*, 3515–3521. [CrossRef]
30. Liu, H.; Bai, J.; Yan, K.; Yan, J.L.; Ma, A.B.; Jiang, J.H. Comparative studies on evolution behaviors of 14H LPSO precipitates in as-cast and as-extruded Mg-Y-Zn alloys during annealing at 773 K. *Mater. Des.* **2016**, *93*, 9–18. [CrossRef]
31. Wu, Y.J.; Lin, D.L.; Zeng, X.Q.; Peng, L.M.; Ding, W.J. Formation of a lamellar 14H-type long period stacking ordered structure in an as-cast Mg-Gd-Zn-Zr alloy. *J. Mater. Sci.* **2009**, *44*, 1607–1612. [CrossRef]
32. Suzuki, M.; Kimura, T.; Koike, J.; Maruyama, K. Effects of zinc on creep strength and deformation substructures in Mg-Y alloy. *Mater. Sci. Eng. A* **2004**, *378–389*, 706–709.

33. Liu, H.; Ju, J.; Yang, X.W.; Yan, J.L.; Song, D.; Jiang, J.H.; Ma, A.B. A two-step dynamic recrystallization induced by LPSO phases and its impact on mechanical property of severe plastic deformation processed $Mg_{97}Y_2Zn_1$ alloy. *J. Alloys Compd.* **2017**, *704*, 509–517. [CrossRef]
34. Liu, W.; Ma, Y.B.; Zhang, Y.G.; Fan, X.X.; Xu, C.X.; Zhang, J.S. Two dynamic recrystallization processes in a high-performance extruded $Mg_{94.5}Y_2Gd_1Zn_2Mn_{0.5}$ alloy. *Mater. Sci. Eng. A* **2017**, *690*, 132–136. [CrossRef]
35. Abe, E.; Kawamura, Y.; Hayashi, K.; Inoue, A. Long-period ordered structure in a high-strength nanocrystalline Mg-1 at% Zn-2 at% Y alloy studied by atomic-resolution Z-contrast STEM. *Acta Mater.* **2002**, *50*, 3845–3857. [CrossRef]
36. Hagihara, K.; Yokotani, N.; Umakoshi, Y. Plastic deformation behavior of $Mg_{12}YZn$ with 18R long-period stacking ordered structure. *Intermetallics* **2010**, *18*, 267–276. [CrossRef]
37. Shao, X.H.; Yang, Z.Q.; Ma, X.L. Strengthening and toughening mechanisms in Mg-Zn-Y alloy with a long period stacking ordered structure. *Acta Mater.* **2010**, *58*, 4760–4771. [CrossRef]
38. Xu, C.; Nakata, T.; Qiao, X.G.; Zheng, M.Y.; Wu, K.; Kamado, S. Ageing behavior of extruded Mg-8.2Gd-3.8Y-1.0Zn-0.4Zr (wt %) alloy containing LPSO phase and γ' precipitates. *Sci. Rep.* **2017**, *7*, 43391. [CrossRef] [PubMed]
39. Rong, W.; Wu, Y.J.; Zhang, Y.; Sun, M.; Chen, J.; Peng, L.M.; Ding, W.J. Characterization and strengthening effects of γ' precipitates in a high-strength casting Mg-15Gd-1Zn-0.4Zr (wt %) alloy. *Mater. Charact.* **2017**, *126*, 1–9. [CrossRef]
40. Nie, J.F. Precipitation and hardening in magnesium alloys. *Metall. Mater. Trans. A* **2012**, *43*, 3891–3939. [CrossRef]
41. Yu, Z.J.; Huang, Y.D.; Mendis, C.L.; Hort, N.; Meng, J. Microstructural evolution and mechanical properties of Mg-11Gd-4.5Y-1Nd-1.5Zn-0.5Zr alloy prepared via pre-ageing and hot extrusion. *Mater. Sci. Eng. A* **2015**, *624*, 23–31. [CrossRef]